DOI: 10.1002/((please add manuscript number))
Article type: Communication

Ionic signal amplification of DNA in a nanopore

Makusu Tsutsui,[1,] Kazumichi Yokota,[2] Yuhui He,[3] and Tomoji Kawai[1,*]*

Prof. Makusu Tsutsui, Prof. Tomoji Kawai
The Institute of Scientific and Industrial Research, Osaka University, Mihogaoka 8-1, Ibaraki, Osaka 567-0047, Japan

Dr. Kazumichi Yokota
National Institute of Advanced Industrial Science and Technology, Takamatsu, Kagawa 761-0395, Japan

Pro. Yuhui He
Huazhong University of Science and Technology, Wuhan 430074, China

E-mail: tsutsui@sanken.osaka-u.ac.jp, kawai@sanken.osaka-u.ac.jp

Keywords: nanopore, ionic amplification, permittivity gradient, translocation dynamics, nanofluidics

Ionic signal amplification is a key challenge for single-molecule analyses by solid-state nanopore sensing. Here we report a permittivity gradient approach for amplifying ionic blockade characteristics of DNA in a nanofluidic channel. The transmembrane ionic current response was found to change substantially through modifying the liquid permittivity at one side of a pore with an organic solvent. Imposing positive liquid permittivity gradients with respect to the direction of DNA electrophoresis, we observed the resistive ionic signals to become larger due to the varying contributions of molecular counterions. On contrary, negative gradients rendered adverse effects thereby causing conductive ionic current pulses upon polynucleotide translocations. Most importantly, both the positive and negative gradients were demonstrated to be capable of amplifying the ionic signals by an order of magnitude with 1.3-fold difference in the transmembrane liquid dielectric constants. This phenomenon allows a novel way to enhance the single-molecule sensitivity of nanopore

sensing that may be useful in analyzing secondary structures and genome sequence of DNA by ionic current measurements.

Ion flow in nanofluidic channels is a fundamental yet pivotal process in a wide range of cellular functions that are programmed to amplify and transduce ionic signals in response to external stimuli via ingenious molecular mechanisms.[1-3] Advance in semiconductor technologies has led to growing interest in mimicking and exploiting the structure and rich ionic characteristics of biological pores by allowing a way to sculpt a nanoscale hole in a dielectric membrane.[4-8] Single-molecule sequencing has been a central topic for realizing high-throughput genome analyses[4] to organic memory systems[9] that implements cross-membrane ionic current measurements to detect distinct differences in ion blockade characteristics of the four nucleotides. However, the fast translocation motion of polynucleotides remains a challenge to readout the genome sequence.[10-12] The intrinsically weak ionic signals[13] due to the intriguing roles of DNA counterions[14] also pose difficulties to attain single-base resolution. Sequencing by solid-state nanopore sensing is, therefore, yet to be an affordable technology.

We herein report on a simple approach for simultaneous implementation of ionic blockade signal amplification and translocation deceleration of polynucleotides in a nanopore. Our system consisted of a nanopore in a SiN_x membrane interfacing 0.69 M NaCl water-glycerol mixture solutions of viscosities η_{cis} and η_{trans} (Figure 1a).[15] The miscible liquids were chosen to simplify the problem by avoiding the intriguing influence of liquid-liquid interfacial properties such as junction potential and surface tension.[16-19] The ionic current I_{ion} through a 100 nm diameter pore scaled linearly with the transmembrane voltage V_b when there was no viscosity difference at the *cis* and *trans* (Figure 1b). When $\eta_{cis} > \eta_{trans}$, on the other hand, the $I_{ion} - V_b$ curves showed an asymmetric feature exhibiting lower nanopore conductance at the negative voltages. This is interpreted as a consequence of the electroosmosis-derived hydrodynamic flow in the *trans*-to-*cis* (*cis*-to-*trans*) direction under positive (negative) V_b that tends to decrease (increase) the liquid viscosity by filling the pore with more water

(glycerol),[20] as also revealed to be the case for the present SiN_x nanopore in the framework of finite element analyses (Figures 1c and 1d).

We recorded the ionic current through the pore under the applied transmembrane voltage of 0.3 V with double-stranded DNA (48.5 kbp) added to *cis*. When the measurement was conducted in water, the electric field focused at the nanopore drew the negatively-charged biopolymers causing small dips in the I_{ion} trace. A close look into the signals revealed square wave-like profiles characteristic of the long string-like molecules.[21] On the other hand, formations of a two-phase system by replacing one side of the water with glycerol solution led to a marked change in the ionic current signatures, where we denoted the liquid arrangements by the viscosity ratio $r_{vis} = \eta_{cis}/\eta_{trans}$ (Figure 2a). Adding the organic solvent into *trans*, for instance, we found the resistive pulses to become larger. More strikingly, the inclusion of glycerol in *cis* resulted in sign inversion of the I_{ion} signals. Yet their line shapes retained the multi-step feature representing the folding motifs of DNA irrespective of the solution conditions (Figures 2b and 2c),[21-23] which unambiguously suggested a role of the two-phase liquid system to cause dramatic changes in the ionic current blockade characteristics.

No such behavior was found when we homogeneously altered the liquid properties keeping r_{vis} to 1. This can be seen in Figure 3a where we measured the ionic current in a nanopore both sides filled with the same water-glycerol mixture solution. Adding more glycerol in water, we obtained lower open pore current anticipating diminished mobility of ions under larger hydrodynamic dragging in the more viscous media (Figure S1).[24] Consistently, the resistive pulses tended to become smaller and wider with the volume fraction of glycerol as the larger viscous drag forces also served to slow-down the electrophoretic motions of DNA (Figures 3b and 3c).[25] Meanwhile, since neither enhancement nor sign inversion of the ion blockade current was observed, the anomalous

characteristics of the two-phase nanopore is indicated as not a straightforward outcome of the solution viscosity.

The situations were similar for objects other than polynucleotides. In the case of 100 nm-sized carboxylated polymeric beads in a 150 nm diameter pore (Figures 3c and S2-S4), we observed a steady decrease in the resistive pulse height I_p together with the open pore current I_0 with the solution viscosity under $r_{vis} = 1$ (see also Figures S5-S7 for the results of 200 nm nanoparticles). More quantitatively, both I_p and I_0 scaled approximately as η^{-1} (Figures 2c, S2d, and S5c), which is a mere consequence of the viscosity-dependent electrolyte solution resistivity known as Walden's rule.[26] The translocation time of the nanobeads also exhibited the same tendency since their electrophoretic mobility μ varies with η as $\mu = q/3\pi\eta d$, where q is the surface charge of particles of diameter d (Figures S3 and S6). Moreover, the peculiar two-phase nanopore sensing characteristics was not reproduced for the polymeric nanoparticles. Imposing viscosity gradients, we detected weaker resistive pulses attributed to the increased solution resistivity by the overall increase in the liquid viscosity (Figures 3d and 3e; see also Figures S8 and S9). Whether the two-phase liquid systems were actually formed can be confirmed from the asymmetric signal waveforms (Figure S8b)[27] demonstrating transitions from high-to-low (low-to-high) mobility of nanobeads upon the translocation under the imposed positive (negative) viscosity gradients.[28] The peculiar blockade current characteristics seen in Figure 2 is thus indicated as a property intrinsic to DNA.

It is noticeable in this regard that dense counterions on polynucleotides raise the ionic density at a nanopore upon translocation, which counteracts the ion depletion by volume exclusion to even induce current enhancements under a particular condition.[22,23,29] This molecular charge effect becomes more prominent in diluter electrolytes since a larger number of counter-cations, relative to the bulk ion concentration, are provided in the nanochannel due to the longer Debye length (While the counterion contribution influences the ionic blockade

characteristics of the polymeric nanoparticles as well, its effect is anticipated to be only marginal for the much smaller charge density per volume).[30] Analogously, liquid dielectric properties are theoretically predicted to matter on the I_{ion} response for more (less) counterions are attracted on polynucleotides in a solvent of higher (lower) permittivity.[30,31] To verify this, we performed the nanopore sensing in aqueous ethanol (The relative dielectric constants ε of water, glycerol, and ethanol are 80, 47, and 24, respectively). Keeping the ion concentration at 0.69 M, we formed a permittivity gradient across the membrane in a way akin to the measurements in the glycerol solutions (Figure 4). Since the viscosity of ethanol (1.2 mPa·s) is very close to that of water (1.1 mPa·s), we can directly evaluate the contribution of the liquid dielectric properties by profiling the permittivity gradient dependence of the ionic current blockade characteristics.

The nanopore sensing with ethanol gradients indeed elucidated a profound function of the liquid dielectric properties on the I_{ion} response to DNA translocation. We detected larger resistive pulses under negative permittivity gradients, *i.e.* when aqueous ethanol is added to *cis* to make the *cis*-to-*trans* permittivity ratio r_{perm} to be larger than unity (Figures 4a and 4b), where we used Onsager theory[32] to assess the relative dielectric constant of the mixture solutions. Conversely, sign inversion of the pulse signals occurred when $r_{perm} > 1$. The results are in accordance with Figure 2 as the dielectric constant of glycerol is smaller than the water counterpart. Quantitatively, the I_{ion} signal heights under the glycerol and ethanol gradients showed resembling dependence against r_{perm} (Figure 4c) thereby demonstrating the predominant influence of the permittivity gradients on the anomalous I_{ion} response to DNA translocation through two-phase nanopores that amplified the ionic signals by up to an order of magnitude via the 1.3-fold difference in ε.

The underlying mechanism can be depicted by the fact that the electroosmotic flow pushes water into the nanopore when $r_{vis} > 1$ (Figure S10). Since water has relatively larger permittivity compared to glycerol and ethanol, it means longer Debye length λ_D in and around

the nanochannel since $\lambda_D \sim \varepsilon^{0.5}$. This predicts larger contributions of the DNA counterions, which is consistent to the experimental observations of the ionic current enhancements. Conversely, the water pushes the organic solvents into the nanopore for the case of $r_{vis} < 1$ that shortens λ_D, and hence suppresses the counterion effects to bring larger resistive pulses (Figure S11).

Besides the signal enhancement via the permittivity effect, the viscosity gradient in the water-glycerol nanopores enables damping the fast electrophoretic motions of DNA in the nanopore. This can be noticed in Figure 4d where we plotted the average signal width t_d against r_{vis}. It shows up to a factor of two decreases in the translocation speed under the 10-fold viscosity difference, the capability of which would be particularly useful for the nanopore sequencing.[33]

Perhaps the only drawback of the two-phase nanopore approach is the elevated ionic current noise evident in Figures 2a and 4a. This is in sharp contrast to the case when we homogeneously changed the liquid properties that provided lower noise floor under lower ε and higher η (Figure 3a, see also Figure S12). The large I_{ion} fluctuations are hence ascribed to the non-steady nature of the liquid composition in the two-phase liquid system under the ion and electroosmotic flow involved.[28] Fast Fourier analyses disclosed the distinctive roles of permittivity and viscosity (Figures S13 and S14). For instance, ethanol gradients were found to enlarge the high-frequency noise presumably through the capacitance-amplifier source coupling mechanism (Figure 4e inset).[34,35] This ε-dependence was also present in the water-glycerol systems as shown in the plots of the power spectral density ΔI_{10k} at 10 kHz as a function of r_{perm} (Figure 4e inset). In addition to the capacitance contribution, the viscosity gradients raised the low-frequency noise rendering more pronounced $1/f$ components, whose effect was less significant in the water-ethanol nanopore due to the negligible difference in their η (Figure 4e).

An advantage of the permittivity gradient approach lies in its ability to amplify ionic current signals without largely affecting other features relevant to nanopore sensing. This is different from other similar procedures such as salinity[36] and viscosity gradient methods[17] where the open pore conductance is inevitably affected by the associated change in the ion concentration and viscosity thereby often degrading the single-molecule sensitivity. Transmembrane voltage is another example that involves a faster electrophoretic translocation speed of DNA in an effort to enlarge signal intensities. In contrast to these conventional means, the local permittivity conditions allow to tune the ionic blockade current characteristics independently without any critical trade-off except the capacitance-derived fast current fluctuations. While it may hinder to extract fine molecular features in the ionic current signals,[37] there are digital post-processing techniques,[38] such as the ones based on wavelet transforms[39] and deep learning,[40] that are already proven useful to remove the high-frequency noise without compromising the temporal resolution of the ionic current measurements. Together with the capability to simultaneously slowdown the translocation motions of polynucleotides with a viscous liquid, the present method may offer a step closer to the realization of solid-state nanopore sequencing.

Experimental Section

Solid-state nanopore fabrications. A 4-inch silicon wafer both sides coated with 50 nm-thick SiN_x layers was diced into 30 mm × 30 mm chips. One side of the SiN_x was partially removed by reactive ion etching (Samco) with CHF_3 etchant gas through a metal mask. The Si layer was then wet etched in KOH aq. (Wako) at 50 degrees Celsius through the exposed 1 mm × 1 mm square area. As a result, we formed a 50 nm-thick SiN_x membrane. On the membrane, we spin-coated electron beam resist (ZEP520A, Zeon) and baked at 180 degrees Celsius. Subsequently, we delineated a circle of diameter 300 nm or 100 nm by electron beam lithography (125 kV, Elionix). After development, a nanopore was opened by removing the SiN_x via the reactive etching through the resist mask. Finally, the residual resist layer was completely dissolved in N,N-dimethylformamide followed by rinsing in ethanol and acetone.

Ionic current measurements. A nanopore chip was sealed with two polymer blocks made of polydimethylsiloxane (PDMS). These blocks were made by curing PDMS precursor (Sylgard184, Dow) on an SU-8 mold and baked at 80 degrees Celsius. The mold had an I-shaped pattern of sub-millimeter width and height to form a trench on the polymeric blocks that served as a channel to flow sample solution into the nanopore. Prior to the sealing, three holes were punched into the block. After that, the nanopore chip as well as the PDMS were exposed to oxygen plasma for surface activation. They are then swiftly put together for eternal bonding. A mixture solution of PBS and glycerol or ethanol was injected through one of the three holes in the PDMS. Ag/AgCl rods were also inserted into the holes on both sides of the polymer blocks. The ionic current through the nanopore was recorded by pre-amplifying the output current through one of the rods using a custom-designed amplifier

followed by digitizing using a fast digitizer (PXI-5922, NI) and storing in a solid-state drive (PXI-8267, NI) at a 1 MHz sampling rate under the applied transmembrane voltage V_b.

Ionic current signal extractions. Slowly-changing open pore current was offset to zero by subtracting the linearly-fitted components in every 0.5 s region of ionic current curves. Using the offset traces, resistive pulse signals were searched by setting a threshold level slightly above the noise. When I_{ion} was lower than the threshold, the dip was identified by searching the local minimum until the current turned positive. The I_{ion} data 0.005 s before and after the minimal point were defined as a signal region and saved in a separate file. Positive current thresholds were used for datasets containing ionic current enhancement signals. All these processes were performed automatically under a computer program coded in LabVIEW.

Finite element analyses. Finite element simulations of electroosmotic flow and glycerol concentration distributions around a nanopore were conducted in a two-dimensional Cartesian coordinates system. The calculation model consisted of a 300 nm diameter hole in a 50 nm-thick Si_3N_4 membrane of -0.02 C/m^2 surface charge density separating two cylindrical reservoirs of 5 μm-radius and 15 μm-height. One of the reservoirs was filled with 50 % glycerol solution containing 69 mM NaCl while the other side with a salt solution of the same ionic strength but with no glycerol. The electric voltage was added across the membrane by setting the electric potential at one side to 0.3 V or -0.3 V while the other side was grounded. We ran the calculations to estimate the spatial distributions of the fluid flow speed and the glycerol concentrations by simultaneously solving the Poisson equation, continuity equation at steady-state current, Nernst-Planck equation, and Naiver-Stokes equation using the AC/DC, Chemical Reaction Engineering, and Computational Fluid Dynamics (CFD) modules of COMSOL multiphysics 5.4.

Supporting Information
Supporting Information is available from the Wiley Online Library or from the author.

Acknowledgements
This work was supported by the Japan Society for the Promotion of Science (JSPS) KAKENHI Grant Number 22H01926.

Received: ((will be filled in by the editorial staff))
Revised: ((will be filled in by the editorial staff))
Published online: ((will be filled in by the editorial staff))

References

[1] F. J. Sigworth, Structural biology: life's transistors. *Nature* **2003**, *423*, 21-23 (2003).

[2] W. A. Catterall, G. Wisedchaisri, N. Zhen, The chemical basis for electrical signaling. *Nat. Chem. Biol.* **2017**, *13*, 455-463.

[3] R. A. Lucas, C. -Y. Lin, L. A. Baker, Z. S. Siwy, Ionic amplifying circuits inspired by electronics and biology. *Nat. Commun.* **2020**, *11*, 1568.

[4] L. Xue, H. Yamazaki, R. Ren, M. Wanunu, A. P. Ivanov, J. B. Edel, Solid-state nanopore sensors. *Nat. Rev. Mat.* **2020**, *5*, 931-951.

[5] J. A. Alfaro, P. Bohlander, M. Dai, M. Filius, C. J. Howard, X. F. van Kooten, S. Ohayon, A. Pomorski, S. Schmid, A. Aksimentiev, E. V. Anslyn, G. Bedran, C. Cao, M. Chinappi, E. Coyaud, C. Dekker, G. Dittmar, N. Drachman, R. Eelkema, D. Goodlett, S. Hentz, U. Kalathiya, N. L. Kelleher, R. T. Kelly, Z. Kelman, S. H. Kim, B. Kuster, D. Rodriguez-Larrea, S. Lindsay, G. Maglia, E. M. Marcotte, J. P. Marino, C. Masselon, M. Mayer, P. Samaras, K. Sarthak, L. Sepiashvili, D. Stein, M. Wanunu, M. Wilhelm, P. Yin, A. Meller, C. Joo, The emerging landscape of single-molecule protein sequencing technologies. *Nat. Methods* **2021**, *18*, 604-617.

[6] J. P. Fried, J. L. Swett, B. P. Nadappuram, J. A. Mol, J. B. Edel, A. P. Ivanov, J. R. Yates, *In situ* solid-state nanopore fabrication. *Chem. Soc. Rev.* **2021**, *50*, 4974-4992.

[7] Y. He, M. Tsutsui, Y. Zhou, X. -S. Miao, Solid-state nanopore systems: from materials to applications. *NPG Asia Mat.* **2021**, *13*, 48.

[8] Z. Zhang, L. Wen, L. Jiang, Nanofluidics for osmotic energy conversion. *Nat. Rev. Mat.* **2021**, *6*, 622-639.

[9] K. Chen, J. Zhu, U. Keyser, Nanopore-based DNA hard drives for rewritable and secure data storage. *Nano Lett.* **2020**, *20*, 3754-3760.

[10] B. M. Venkatesan, R. Bashir, Nanopore sensors for nucleic acid analysis. *Nat. Nanotechnol.* **2011**, *6*, 615-624.

[11] X. Liu, Y. Zhang, R. Nagel, W. Reisner, W. B. Dunbar, Controlling DNA tug-of-war in a dual nanopore device. *Small* **2019**, *15*, 1701704.

[12] C. Wang, S. Sensale, Z. Pan, S. Senapati, H. -C. Chang, Slowing down DNA translocation through solid-state nanopores by edge-field leakage. *Nat. Commun.* **2021**, *12*, 140.

[13] D. B. Wells, M. Belkin, J. Comer, A. Aksimentiev, Assessing graphene nanopores for sequencing DNA. *Nano Lett.* **2012**, *12*, 4117-4123.

[14] L. S. Lastra, Y. M. Nuwan, D. Y. Bandara, M. Nguyen, N. Farajpour, K. J. Freedman, On the origins of conductive pulse sensing inside a nanopore. *Nat. Commun.* **2022**, *13*, 2186.

[15] N. -S. Cheng, Formula for the viscosity of a glycerol-water mixture. *Ind. Eng. Chem. Res.* **2008**, *47*, 3285-3288.

[16] J. Feng, K. Liu, R. D. Bulushev, S. Khlybov, D. Dumcenco, A. Kis, A. Radenovic, Identification of single nucleotides in MoS_2 nanopores. *Nat. Nanotechnol.* **2015**, *10*, 1070-1076.

[17] S. J. Lee, J. Y. Kang, W. Choi, R. Kwak, Nanopore sensing in aqueous two-phase system: Simultaneous enhancement of signal and translocation time via conformal coating. *Small* **2017**, *13*, 1601725.

[18] M. Shankla, A. Aksimentiev, Molecular transport across the ionic liquid-aqueous electrolyte interface in a MoS_2 nanopore. *ACS Appl. Mater. Interfaces* **2020**, *12*, 26624-26634.

[19] J. S. Lee, J. P. Oviedo, Y. M. N. D. Y. Bandara, X. Peng, L. Xia, Q. Wang, K. Garcia, J. Wang, M. J. Kim, M. J. Kim, Detection of nucleotides in hydrated ssDNA via 2D h-BN nanopore with ionic-liquid/salt-water interface. *Electrophoresis* **2021**, *42*, 991-1002.

[20] Y. Qiu, Z. S. Siwy, M. Wanunu, Abnormal ionic-current rectification caused by reversed electroosmotic flow under viscosity gradients across thin nanopores. *Anal. Chem.* **2019**, *91*, 996-1004.

[21] L. J. Steinbock, O. Otto, C. Chimerel, J. Gornall, U. F. Keyser, Detecting DNA folding with nanocapillaries. *Nano Lett.* **2010**, *10*, 2493-2497.

[22] S. W. Kowalczyk, C. Dekker, Measurement of the docking time of a DNA molecule onto a solid-state nanopore. *Nano Lett.* **2012**, *12*, 4159-4163.

[23] V. Wang, N. Ermann, U. F. Keyser, Current enhancement in solid-state nanopores depends on three-dimensional DNA structure. *Nano Lett.* **2019**, *19*, 5661-5666.

[24] M. Tsutsui, A. Arima, K. Yokota, Y. Baba, T. Kawai, Ionic heat dissipation in solid-state pores. *Sci. Adv.* **2022**, *8*, eabl7002.

[25] D. Fologea, J. Uplinger, B. Thomas, D. S. McNabb, J. Li, Slowing DNA translocation in a solid-state nanopore. *Nano Lett.* **2005**, *5*, 1734-1737.

[26] E. Szwajczak, A. Szymanski, On the relation between mobility of ions and viscosity. The Walden's rule. *Mol. Cryst. Liq. Cryst.* **1986**, *139*, 253-261.

[27] C. Liao, F. Antaw, A. Wuethrich, W. Anderson, M. Trau, Configurable miniaturized 3D pores for robust single-nanoparticle analysis. *Small Structures* **2020**, *1*, 2000011.

[28] S. Marion, N. Vucemilovic-Alagic, M. Spadina, A. Radenovic, From water solutions to ionic liquids with solid-state nanopores as a perspective to study transport and translocation phenomena. *Small* **2021**, *17*, 2100777.

[29] R. M. M. Smeets, U. F. Keyser, D. Krapf, M. -Y. Wu, N. H. Dekker, C. Dekker, Salt dependence of ion transport and DNA translocation through solid-state nanopores. *Nano Lett.* **2006**, *6*, 89-95.

[30] Y. He, M. Tsutsui, C. Fan, M. Taniguchi, T. Kawai, Controlling DNA translocation through gate modulation of nanopore wall surface charges. *ACS Nano* **2011**, *5*, 5509-5518.

[31] M. Zhang, L. -H. Yeh, S. Qian, J. -P. Hsu, S. W. Joo, DNA electrokinetic translocation through a nanopore: Local permittivity environment effect. *J. Phys. Chem. C* **2011**, *5*, 5509-5518.

[32] F. Wang, W. Wang, Y. Jiang, J. Zhu, J. Song, A new model of dielectric constant for binary solutions. *Chem. Eng. Technol.* **2000**, *23*, 623-627.

[33] H. Qiu, W. Zhou, W. Guo, Nanopores in graphene and other 2D materials: A decade's journey toward sequencing. *ACS Nano* **2021**, *15*, 18848-18864.

[34] M. -H. Lee, A. Kumar, K. -B. Park, S. -Y. Cho, H. -M. Kim, M. -C. Lim, Y. -R. Kim, K. -B. Kim, A low-noise solid-state nanopore platform based on a highly insulating substrate. *Sci. Rep.* **2014**, *4*, 7448.

[35] A. Balan, B. Machielse, D. Niedzwiecki, J. Lin, P. Ong, R. Engelke, K. L. Shepard, M. Drndic, Improving signal-to-noise performance for DNA translocation in solid-state nanopores at MHz bandwidths. *Nano Lett.* **2014**, *14*, 7215-7220.

[36] M. Wanunu, W. Morrison, Y. Rabin, A. Y. Grosberg, A. Meller, Electrostatic focusing of unlabelled DNA into nanoscale pores using a salt gradient. *Nat. Nanotechnol.* **2010**, *5*, 160-165.

[37] C. -C. Chien, S. Shekar, D. J. Niedzwiecki, K. L. Shepard, M. Drndic, Single-stranded DNA translocation recordings through solid-state nanopores on glass chips at 10 MHz measurement bandwidth. *ACS Nano* **2019**, *13*, 10545-10554.

[38] C. Wen, D. Dematties, S. -L. Zhang, A guide to signal processing algorithms for nanopore sensors. *ACS Sens.* **2021**, *6*, 3536-3555.

[39] S. Shekar, C. -C. Chien, A. Hartel, P. Ong, O. B. Clarke, A. Marks, M. Drndic, K. L. Shepard, Wavelet denoising of high-bandwidth nanopore and ion-channel signals. *Nano Lett.* **2019**, *19*, 1090-1097.

[40] M. Tsutsui, T. Takaai, K. Yokota, T. Kawai, T. Washio, Deep learning-enhanced nanopore sensing of single-nanoparticle translocation dynamics. *Small Methods* **2021**, *5*, 2100191.

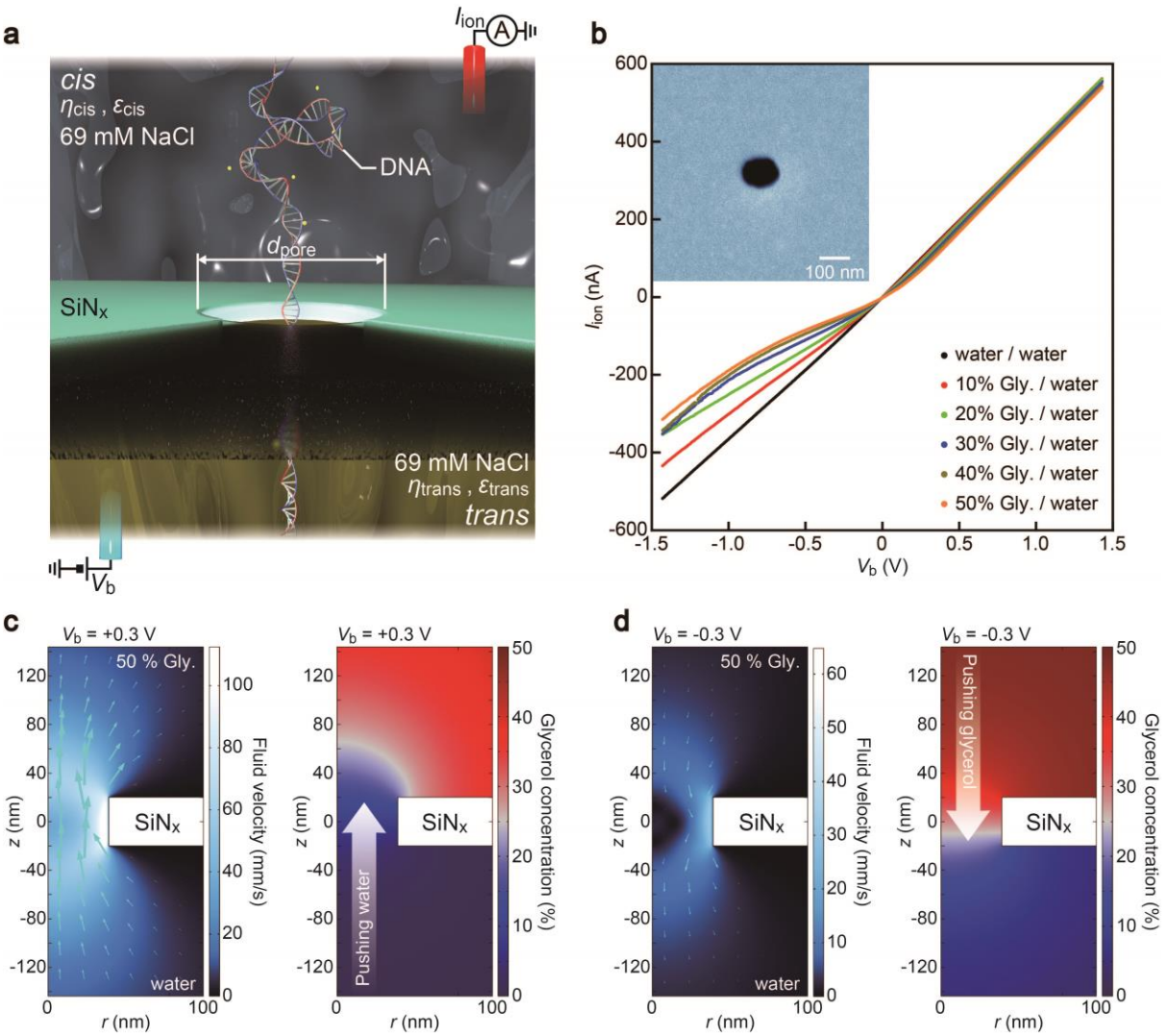

Figure 1. Two-phase nanopore. **a,** A schematic model of DNA translocation through a nanopore of diameter d_{pore} in a 50 nm-thick SiN_x membrane under the applied voltage V_b. The *cis* and *trans* chambers are filled with glycerol solutions of different viscosity $\eta_{cis,trans}$ and permittivity $\varepsilon_{cis,trans}$ but the same salt concentration of 69 mM NaCl. **b,** The ionic current I_{ion} measured under V_b scans. Inset is a scanning electron micrograph of a 100 nm-sized nanopore used. The I_{ion}-V_b curves become asymmetric with respect to the bias polarity showing lower nanopore conductance under negative voltage. **c-d,** Finite element simulations of water flow speed (left) and the glycerol concentration distributions (right) under V_b = +0.3 V (c) and -0.3 V (d). The direction and velocity of the electroosmotic flows are described by the arrows of different sizes. The *trans* and *cis* compartments were filled with water and 50% glycerol solution, respectively. The surface charge density at the SiNx surface was -0.02 C/m^2 causing *trans*-to-*cis* and *cis*-to-*trans* water flow by electroosmosis under positive and negative transmembrane voltages.

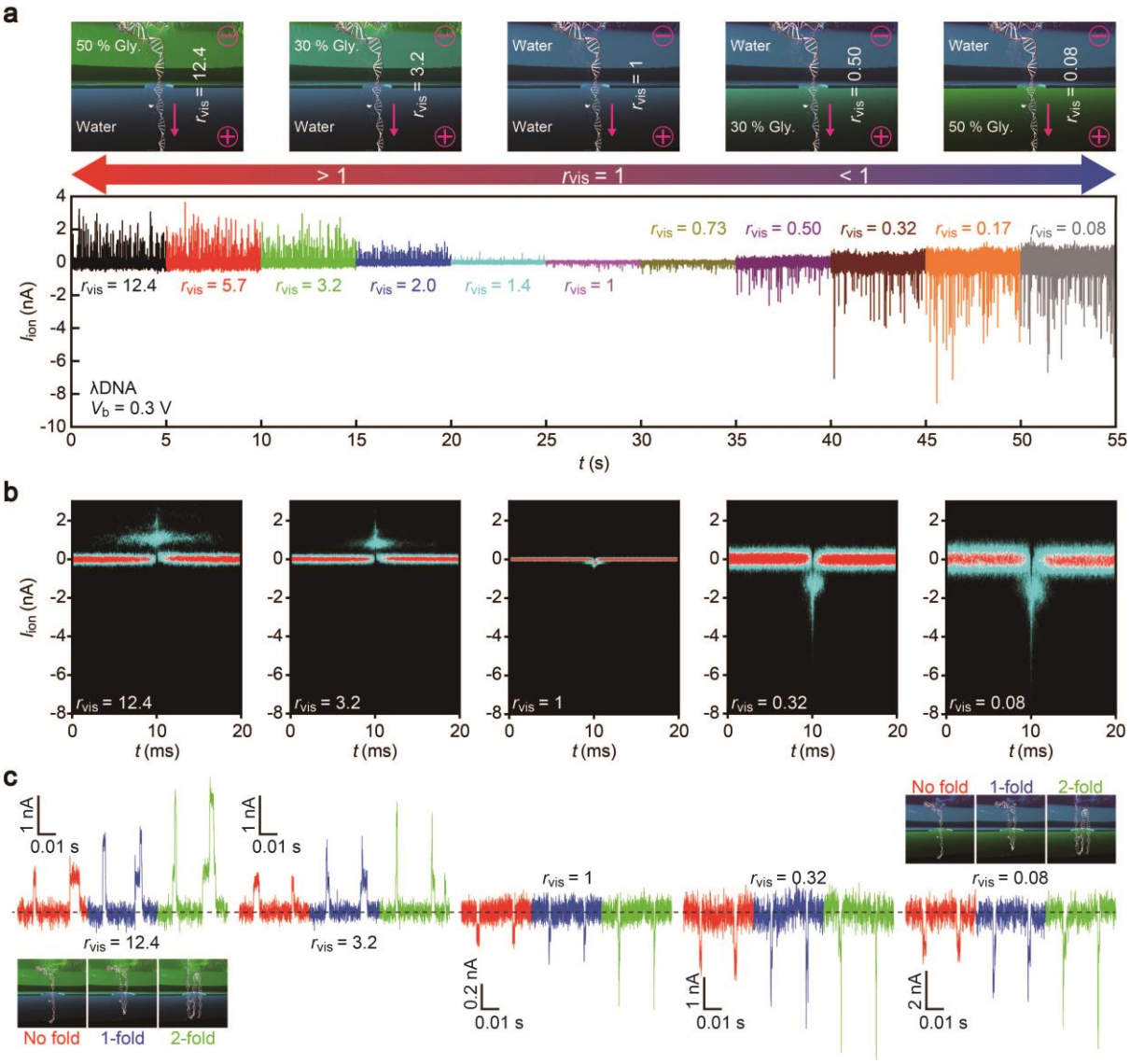

Figure 2. Ion blockade current characteristics of DNA in a water-glycerol nanopore. a, Ionic current traces recorded with a 100 nm-sized two-phase nanopore in a 50 nm-thick SiN_x membrane under the cross-membrane voltage V_b of 0.3 V. *cis* and *trans* are filled with water-glycerol mixture solutions (containing 0.69 M NaCl) to create a viscosity gradient $r_{vis} = \eta_{cis}/\eta_{trans}$. The voltage was in the direction to electrophoretically draw DNA in *cis* into the pore. Note the change in sign of the ionic current (I_{ion}) signals under different r_{vis}. **b,** Two-dimensional histograms of the DNA-translocation-derived I_{ion} signals. **c,** Typical I_{ion} signal waveforms. The dashed line points to zero current. The single- (red), double- (blue), and triple-step features (green) represent the conformations of polynucleotides with no fold, one fold, and two folds, respectively.

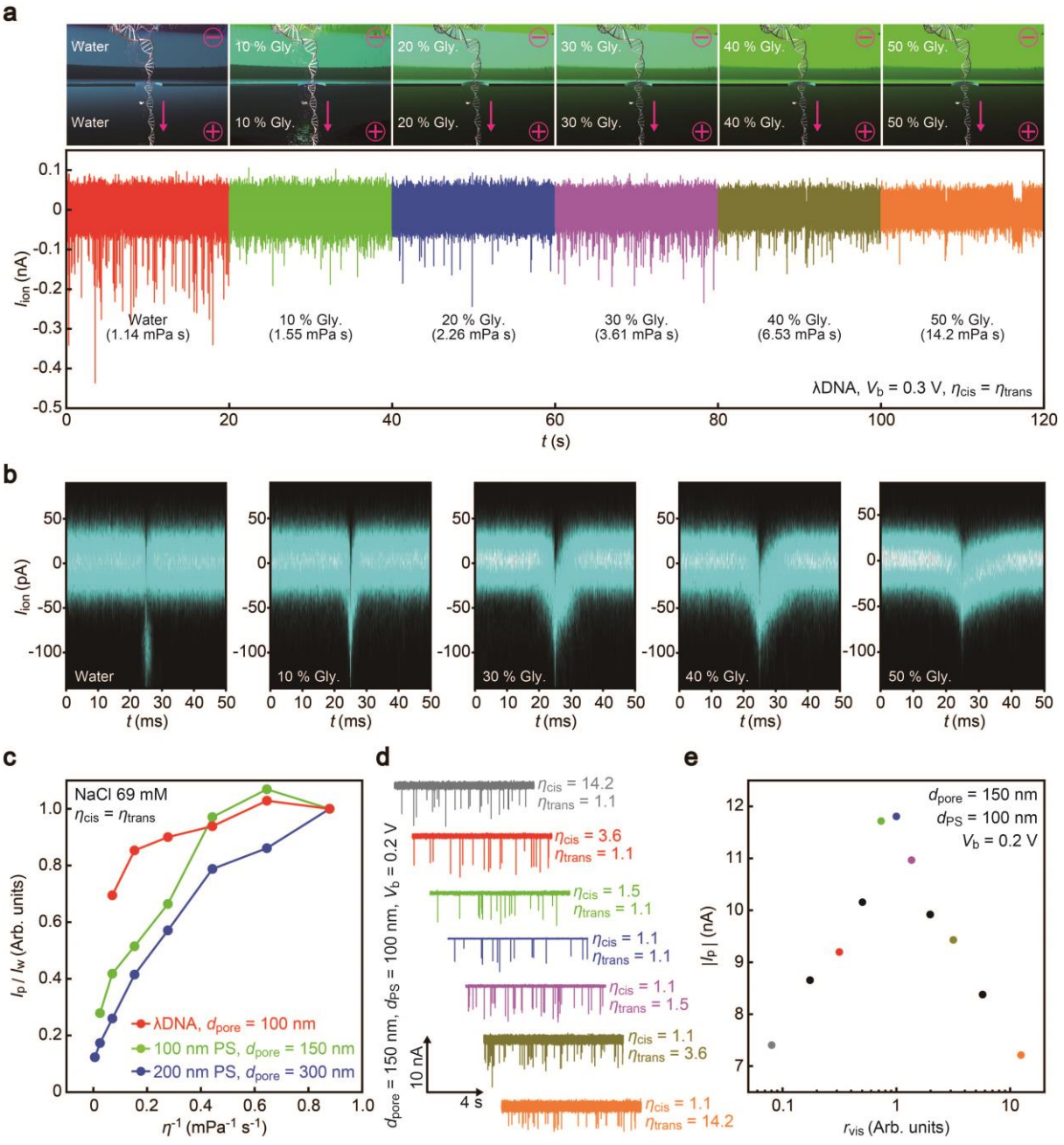

Figure 3. Ionic blockade current characteristics in one-phase nanopores. a, Ionic current traces measured with a 100 nm diameter pore under no viscosity gradients. Resistive pulses were observed indicating electrophoretic translocation of DNA added to *cis* under the transmembrane voltage of 0.3 V. **b,** Two-dimensional histograms of the pulse signals displaying a steady decrease in the intensities with increasing viscosity. **c,** The average signal height I_p plotted as a function of the inverse viscosity η^{-1}. Data are down-sampled to 10 kHz to show the traces at a long time scale. Red, green, and blue plots are data of λDNA, 100 nm polystyrene beads (PS), and 200 nm PS, respectively. I_p is normalized by that in water I_w. **d,** Ionic current curves recorded for 100 nm PS with a water-glycerol nanopore. **e,** The average pulse height in (d) plotted against the viscosity gradient r_{vis}.

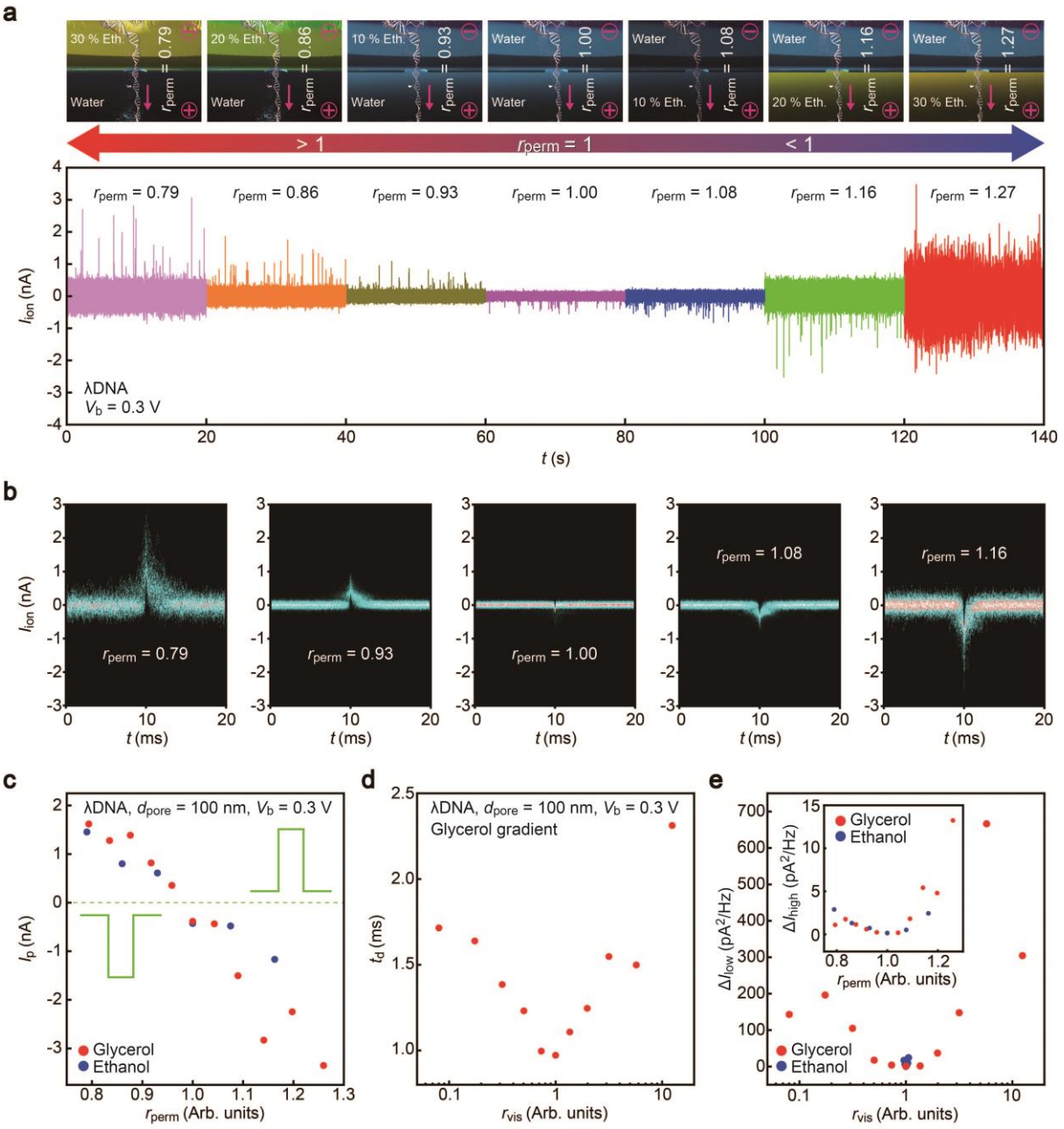

Figure 4. Permittivity-gradient-mediated ionic signal enhancements in two-phase nanopores. **a,** Ionic traces in a two-phase nanopore formed with aqueous ethanol. r_{perm} denotes the permittivity ratio between *cis* and *trans*. **b,** Two-dimensional histograms of ionic current signals. **c,** r_{perm}-dependent I_{ion} pulse height. Red and blue plots are I_p of λDNA in water-glycerol and water-ethanol nanopores. **d,** I_{ion} signal width t_d plotted with respect to r_{vis} for λDNA in a water-glycerol nanopore. **e,** Low frequency noise intensity ΔI_{low} at 100 Hz plotted as a function of r_{vis} for water-glycerol (red) and water-ethanol nanopores (blue). Inset shows r_{perm}-dependent high-frequency noise ΔI_{high} at 10^4 Hz.

Ionic signal amplification of DNA in a nanopore

Makusu Tsutsui, Kazumichi Yokota, Yuhui He, Tomoji Kawai

Keywords: nanopore, permittivity gradient, noise, translocation dynamics, nanofluidics

Makusu Tsutsui, Kazumichi Yokota, Yuhui He, Tomoji Kawai

Local liquid permittivity gradient can amplify ionic signals of DNA in solid-state nanopores.

Supporting Information

Ionic signal amplification of DNA in a nanopore

Makusu Tsutsui, Kazumichi Yokota, Yuhui He, Tomoji Kawai

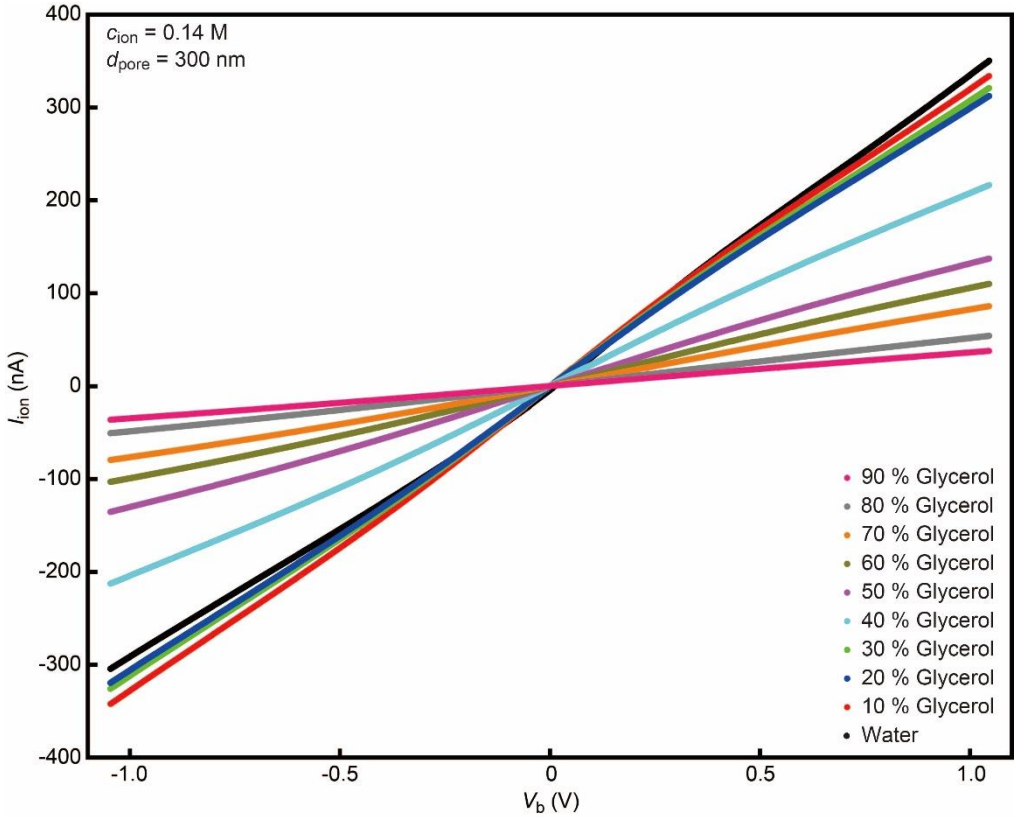

Figure S1. Open pore conductance in water-glycerol mixture solution. Phosphate buffered saline of 1.37 M NaCl concentration was mixed with ultrapure water and glycerol to prepare electrolyte solution of various viscosity but the same salt concentration at 317 mM. The mixture solution of a specific viscosity was added to both sides of a 300 nm-sized nanopore in a 50 nm-thick SiN_x membrane. The ionic current I_{ion} through the pore was measured under voltage sweeps (V_b) from -1 to 1 V. We obtained linear I_{ion}-V_b curves of less steep slopes in the solution of higher viscosity.

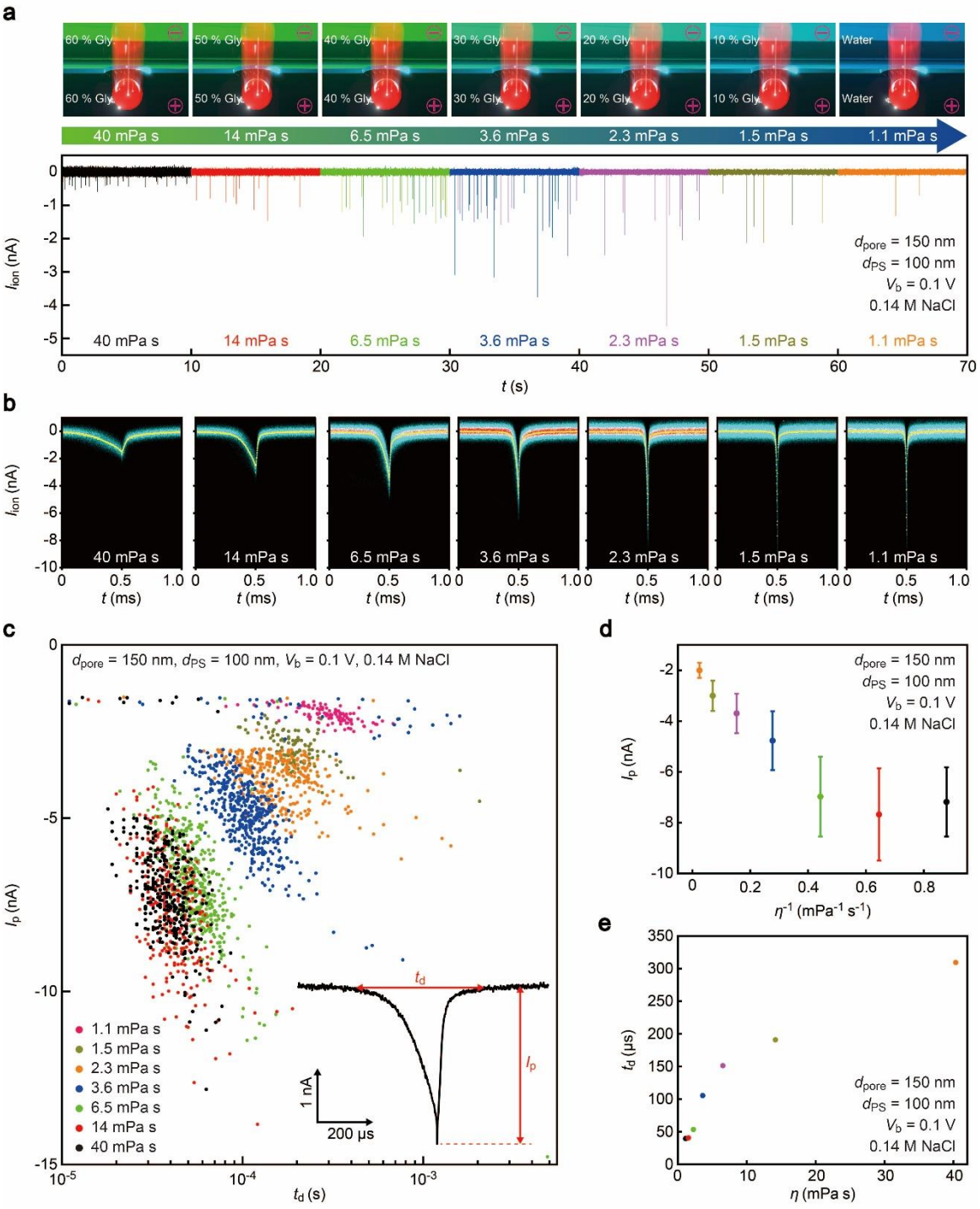

Figure S2. Resistive pulse measurements of 100 nm-sized polystyrene nanobeads in a 150 nm-sized nanopore under homogeneous viscosity conditions at 0.14 M NaCl. **a,** Ionic current curves. Open pore current is offset to zero. The data are down-sampled to 10 kHz. Top images describe the nanopore setup where both sides of the nanopore are filled with the same water-glycerol mixture solution. **b,** Heat maps of resistive pulses obtained under different viscosity conditions. **c,** Resistive pulse height (I_p) versus width (t_d) scatter plots. **d,** I_p plotted as a function of inverse viscosity η^{-1}. **e,** t_d plotted against η.

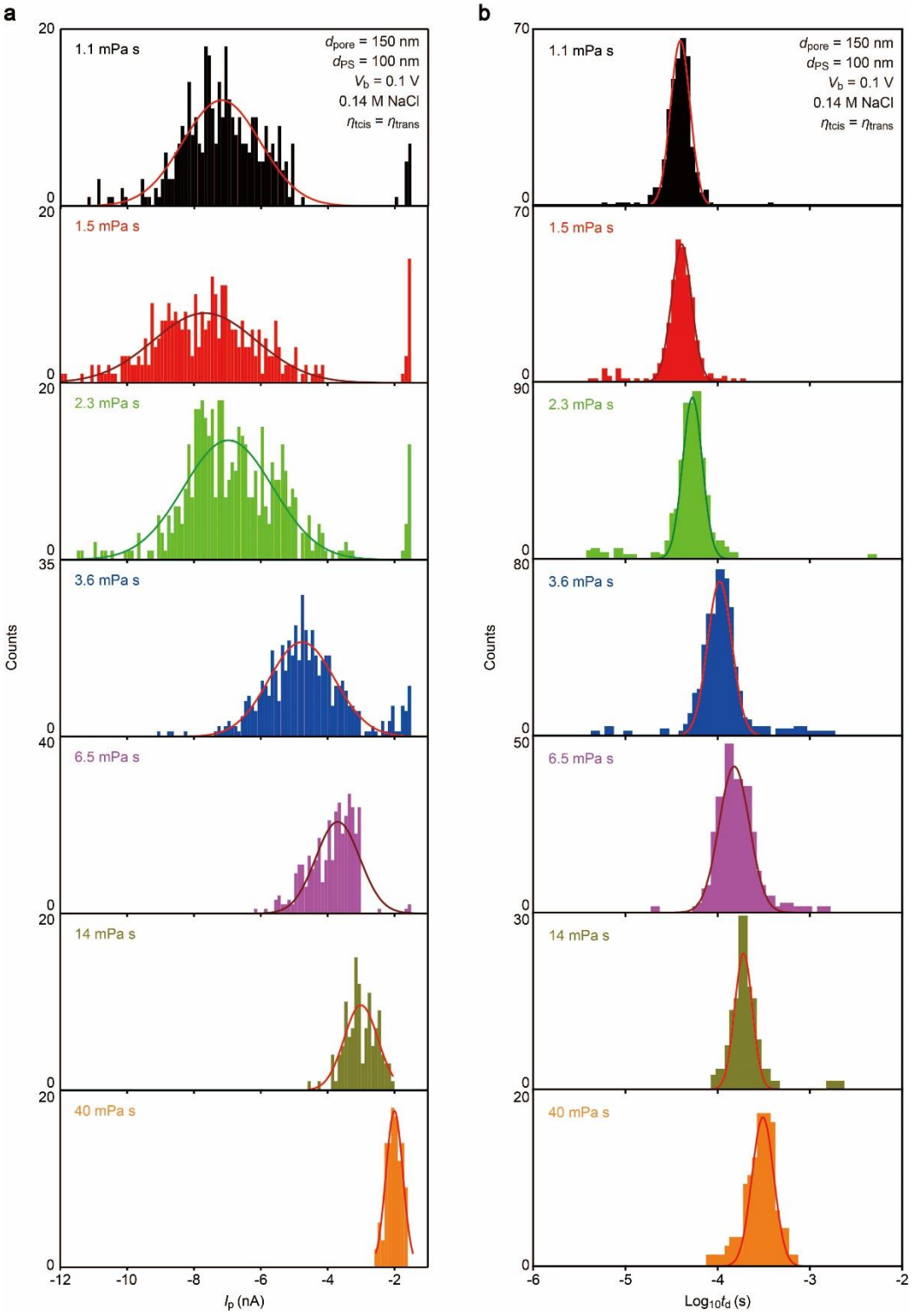

Figure S3. Resistive pulse height and width distributions for 100 nm-sized polystyrene nanobeads translocated through a 150 nm-sized nanopore under homogeneous viscosity conditions. a-b, I_p (a) and t_d (b) histograms. Solid curves are Gaussian fitting to the distributions.

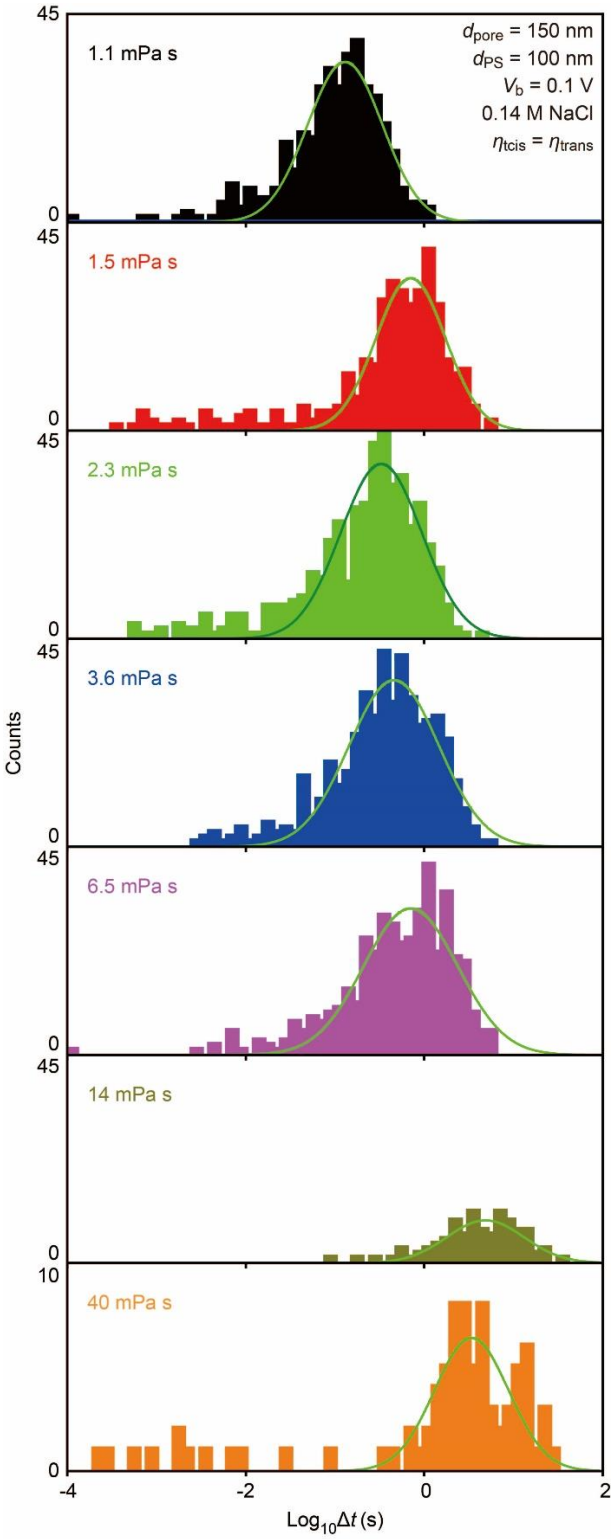

Figure S4. Capture rates of 100 nm-sized polystyrene nanobeads in a 150 nm-sized nanopore under homogeneous viscosity conditions. Δt is the time interval of two ionic current pulse signals. Solid curves are Gaussian fits to the distributions.

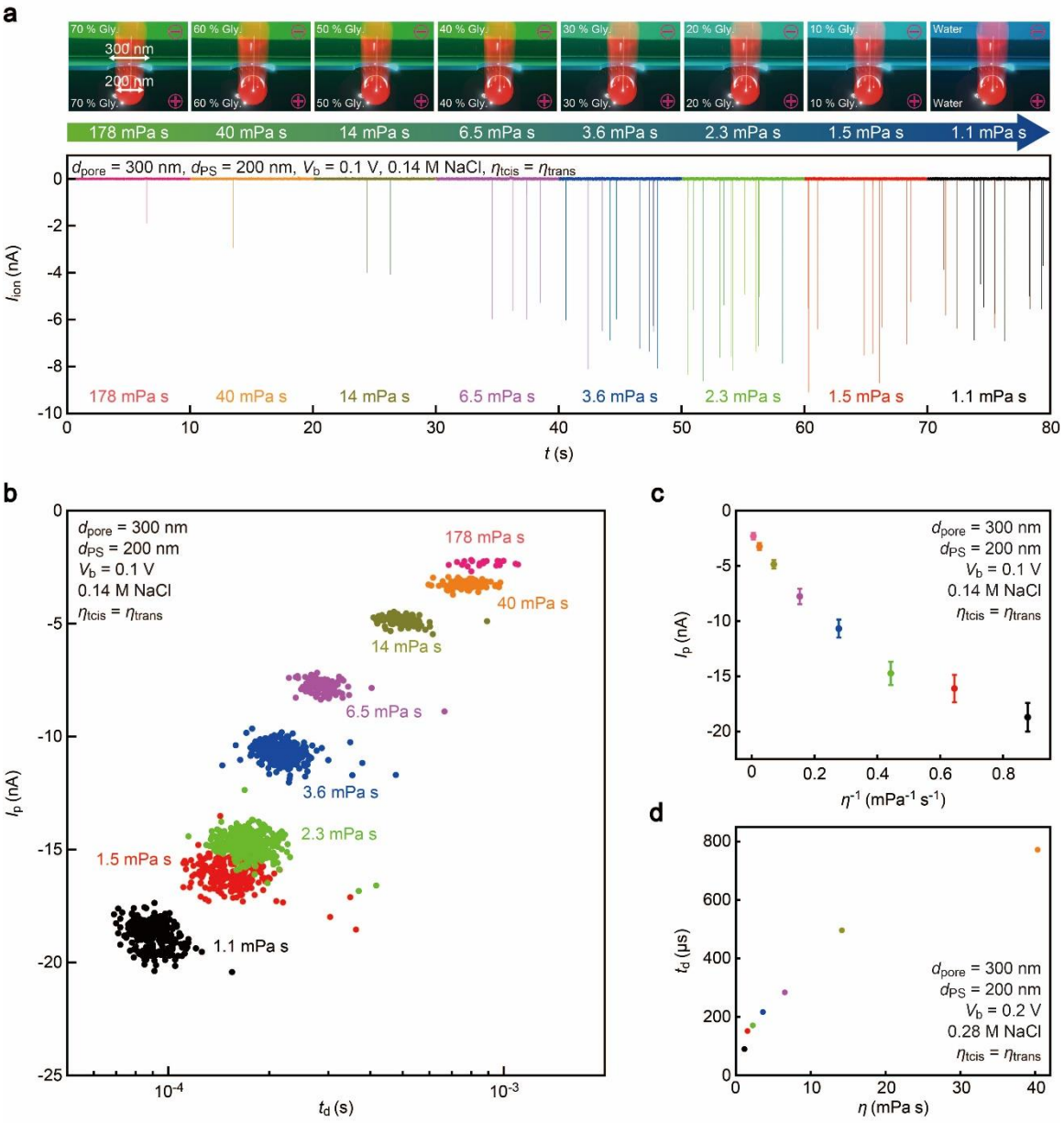

Figure S5. Resistive pulse measurements of 200 nm-sized polystyrene nanobeads in a 300 nm-sized nanopore under homogeneous viscosity conditions at 0.14 M NaCl. **a,** Ionic current curves. Open pore current is offset to zero. The data are down-sampled to 10 kHz. Top images describe the nanopore setup where both sides of the nanopore are filled with the same water-glycerol mixture solution. **b,** Resistive pulse height (I_p) versus width (t_d) scatter plots. **c,** I_p plotted as a function of inverse viscosity η^{-1}. **d,** t_d plotted against η.

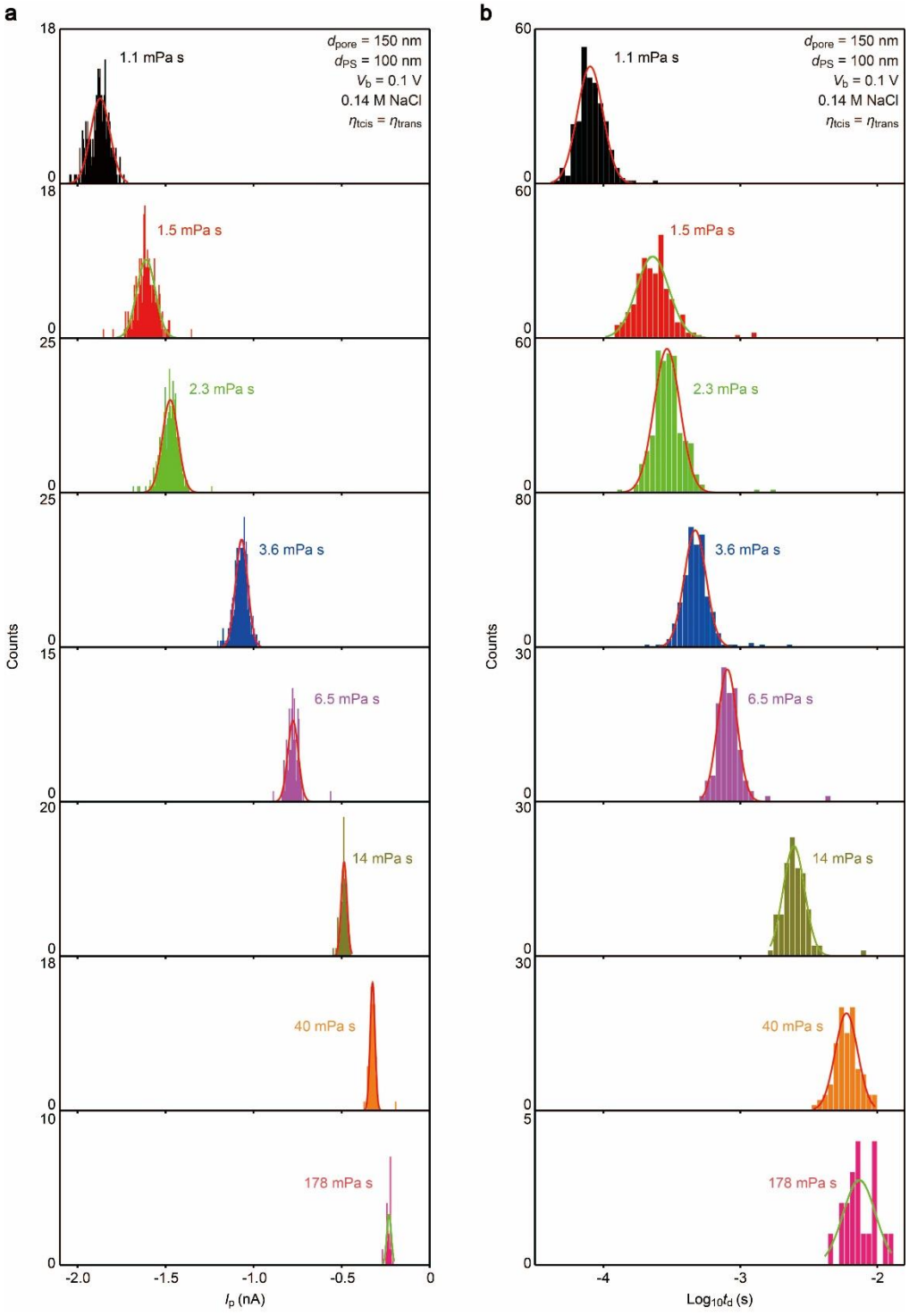

Figure S6. Resistive pulse height and width distributions for 200 nm-sized polystyrene nanobeads translocated through a 300 nm-sized nanopore under homogeneous viscosity conditions. a-b, I_p (a) and t_d (b) histograms. Solid curves are Gaussian fits to the distributions.

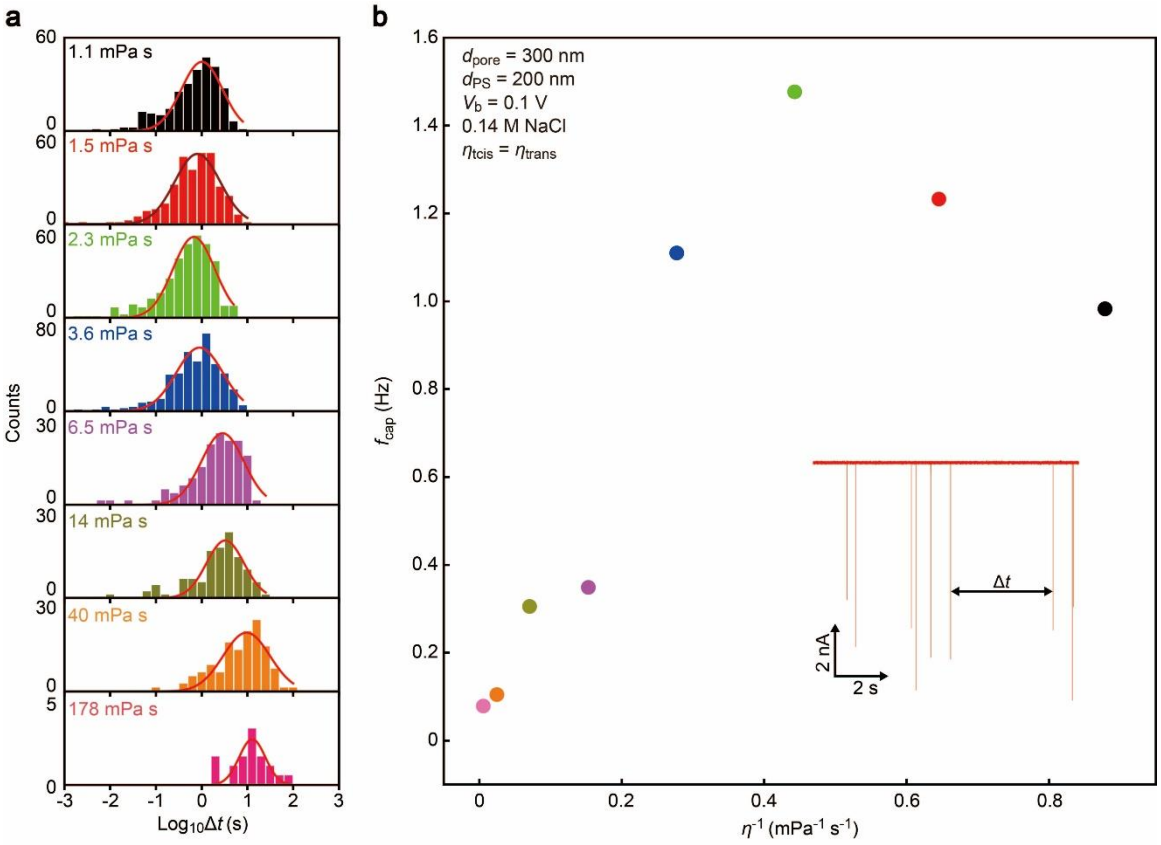

Figure S7. Capture rates of 200 nm-sized polystyrene nanobeads in a 300 nm-sized nanopore under homogeneous viscosity conditions. a, Histograms of $\log_{10}\Delta t$ under different solution viscosities. Solid curves are Gaussian fits to the distributions. **b,** Capture rates $f_{cap} = 1/\Delta t$ plotted with respect to the inverse viscosity η^{-1}. Inset shows the definition of Δt.

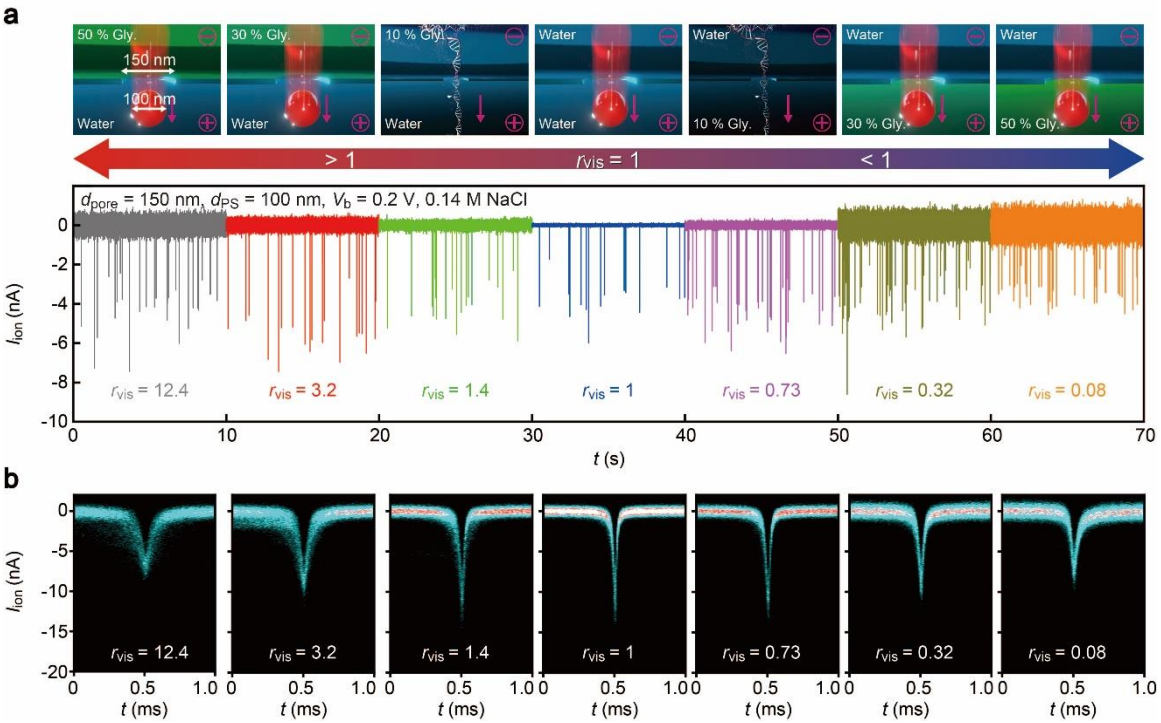

Figure S8. Resistive pulse measurements of 100 nm-sized polystyrene nanobeads in a 150 nm-sized nanopore under viscosity gradients at 0.14 M NaCl. **a,** Ionic current curves. The data are down-sampled to 10 kHz. Top images describe the nanopore setup where both sides of the nanopore are filled with two different water-glycerol mixture solutions that render a trans-membrane viscosity gradient (expressed as $r_{vis} = \eta_{cis}/\eta_{trans}$). **b,** Heat maps of resistive pulses obtained under different viscosity gradients.

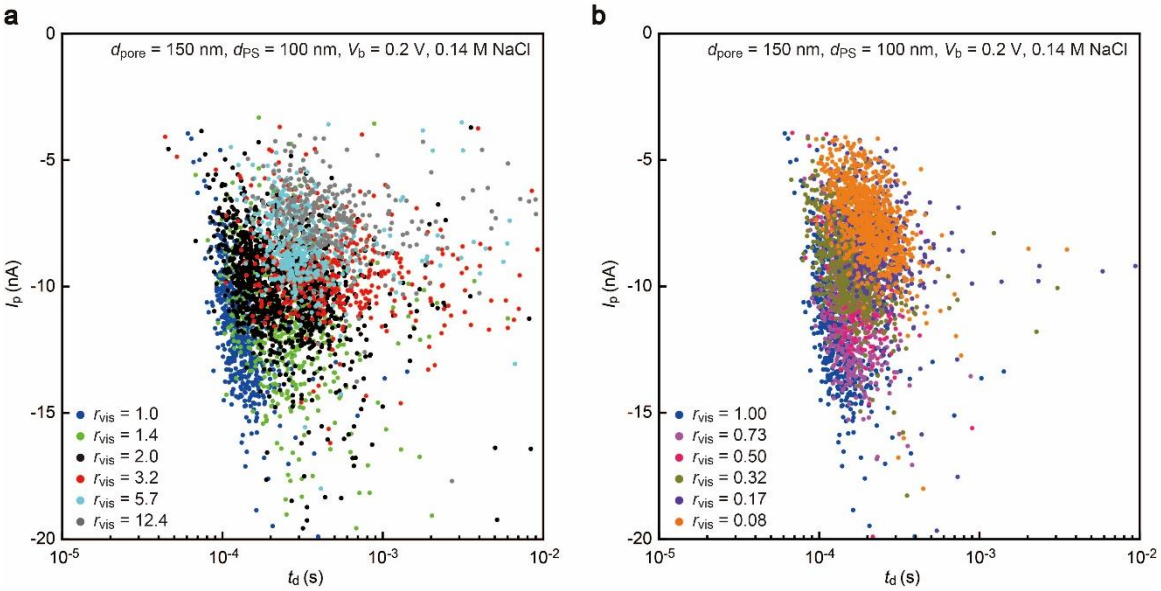

Figure S9. Resistive pulse waveforms of 100 nm-sized polystyrene nanobeads translocated through a 150 nm-sized nanopore under viscosity gradients at 0.14 M NaCl. a-b, I_p versus t_d scatter plots under negative (a) and positive (b) viscosity gradients.

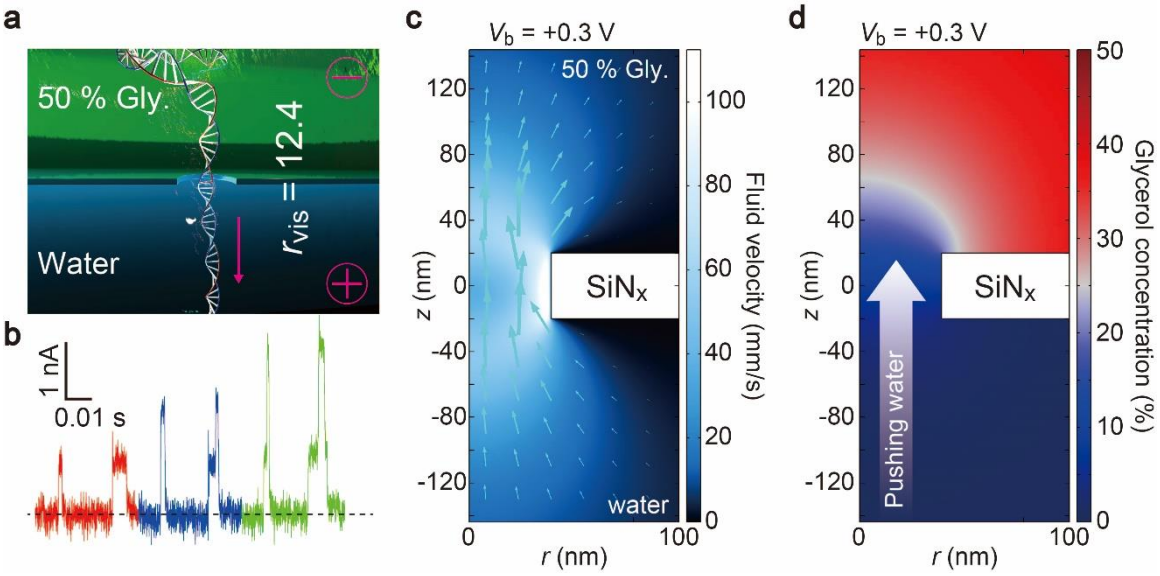

Figure S10. Ionic current enhancements under the viscosity gradient r_{vis} larger than 1. a, Schematic model depicting the measurements of ionic blockade current of DNA under a viscosity gradient where one side of the chamber was filled with 50 % glycerol solution. **b,** Typical ionic current enhancement signals obtained under the condition depicted in (a) with the applied voltage of 0.3 V and the NaCl concentration of 0.69 M. **c,** Finite element analysis of the velocity of the water flow induced by electroosmosis under the condition in (a). **d,** Spatial distribution of glycerol. The electroosmotic flow pushes water to make the local glycerol concentration lower in the nanopore.

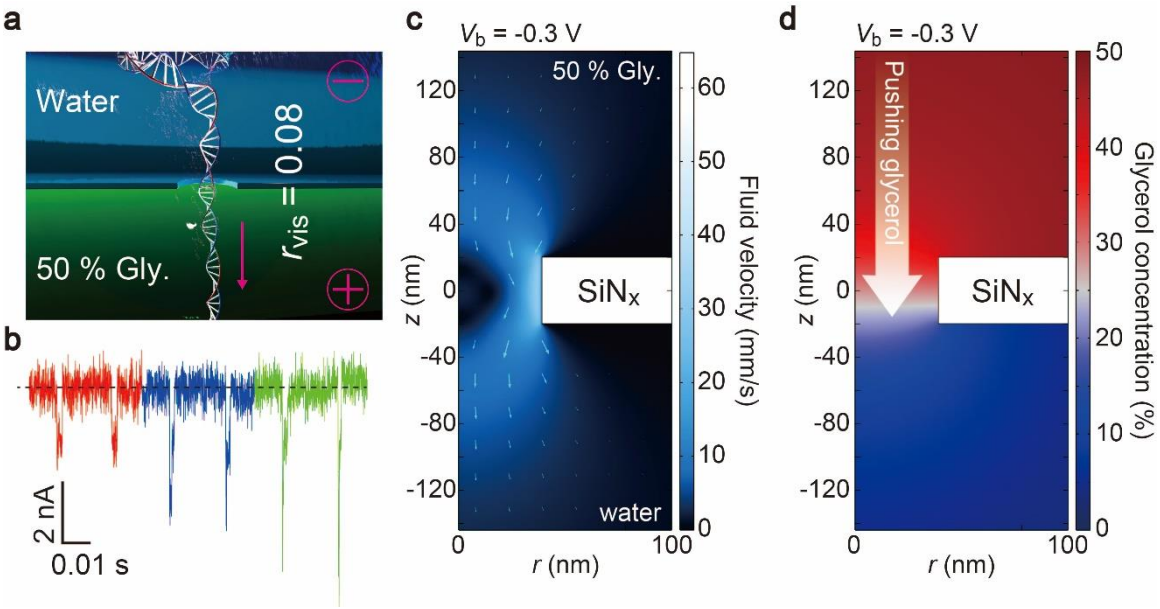

Figure S11. Ionic current enhancements under the viscosity gradient r_{vis} smaller than 1. **a,** Schematic model depicting the measurements of ionic blockade current of DNA under a viscosity gradient where one side of the chamber was filled with 50 % glycerol solution. **b,** Typical resistive pulse signals obtained under the condition depicted in (a) with the applied voltage of 0.3 V and the NaCl concentration of 0.69 M. **c,** Finite element analysis of the velocity of the water flow induced by electroosmosis under the condition in (a). **d,** Spatial distribution of glycerol. The electroosmotic flow pushes glycerol to make its local concentration higher in the nanopore.

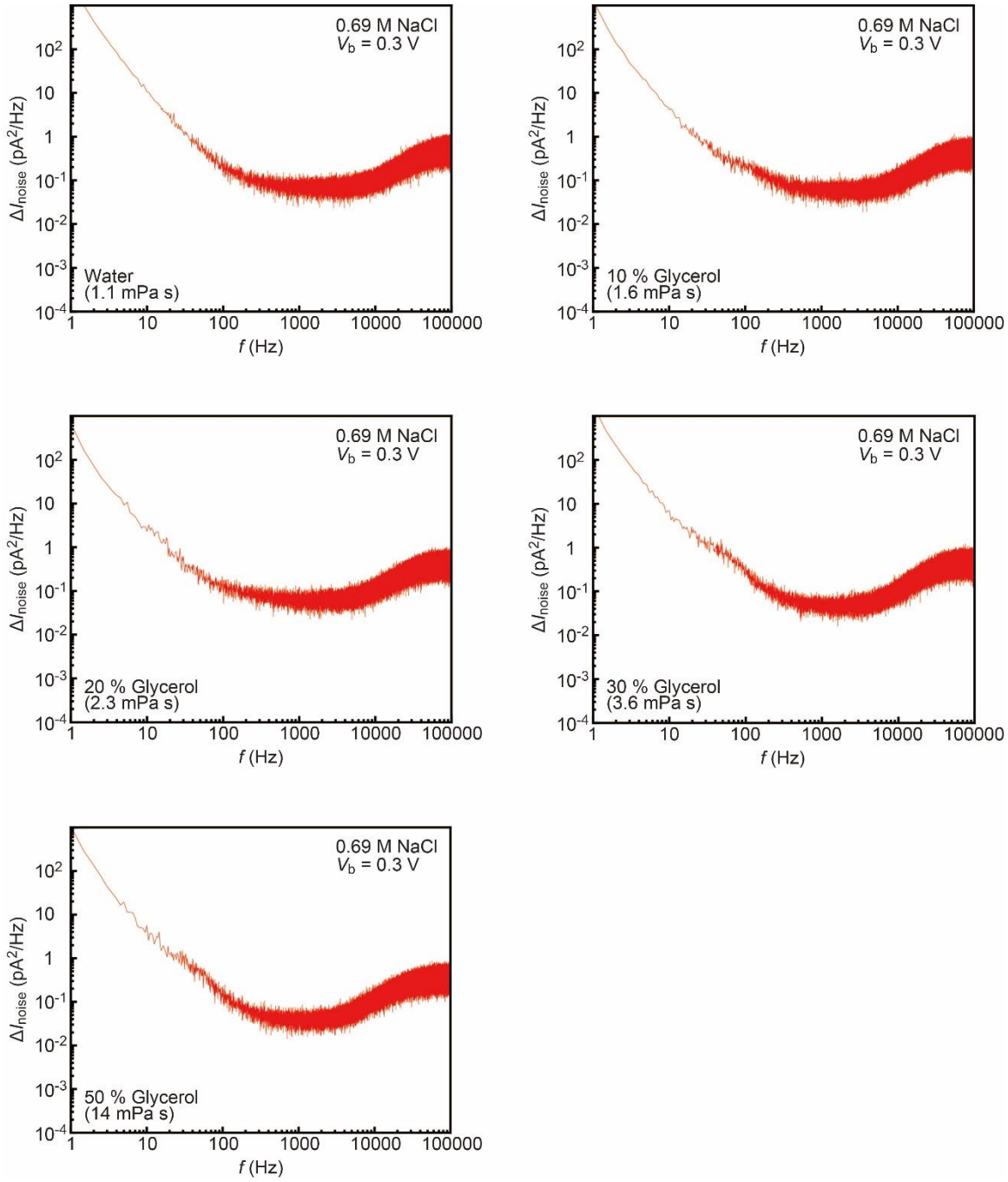

Figure S12. Ionic current noise spectra in a 100 nm-sized nanopore under homogeneous viscosity conditions at 0.69 M NaCl.

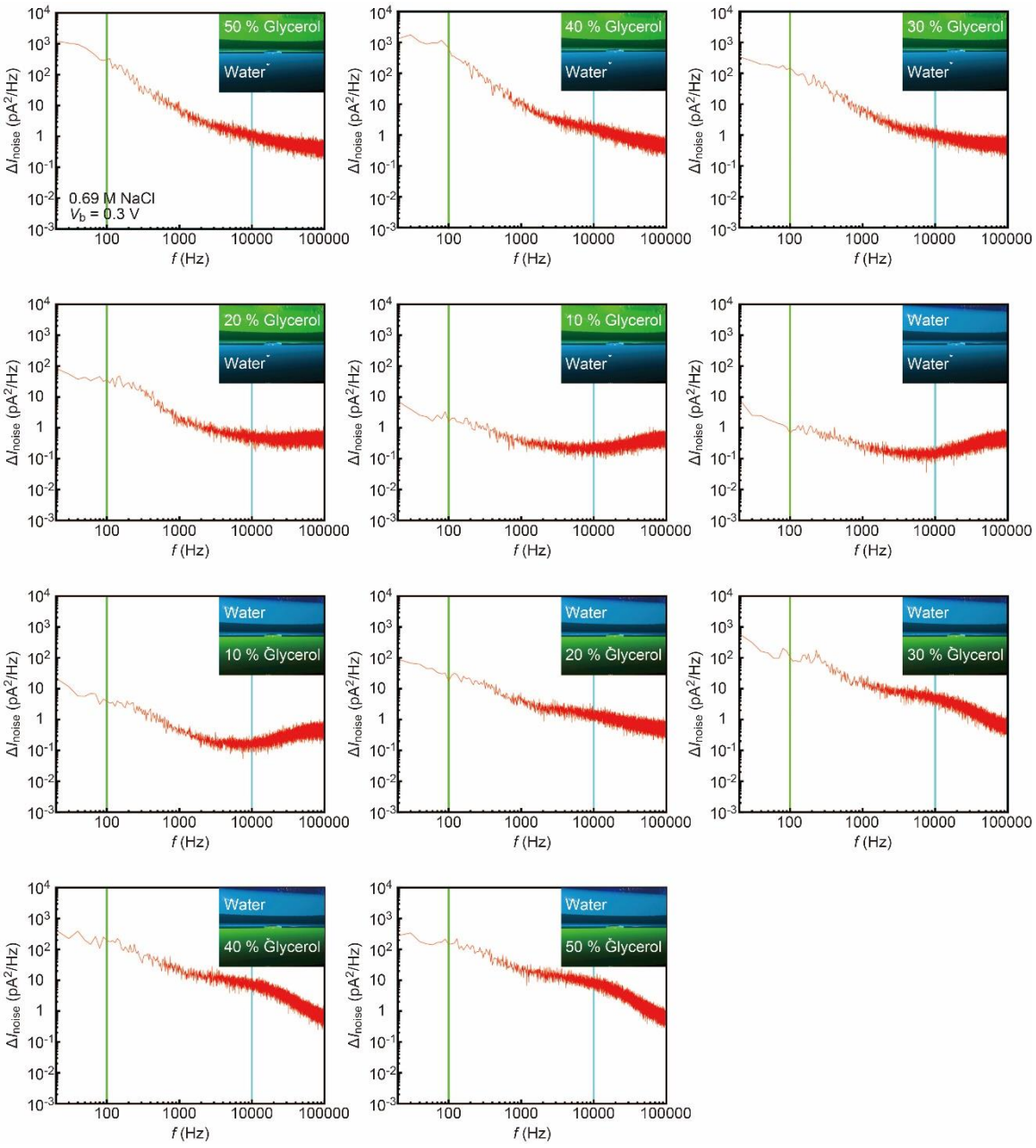

Figure S13. Ionic current noise spectra in a 100 nm-sized nanopore under glycerol gradients at 0.69 M NaCl. Green and blue lines point to the noise intensities at the frequency f = 100 Hz and 10000 Hz, respectively.

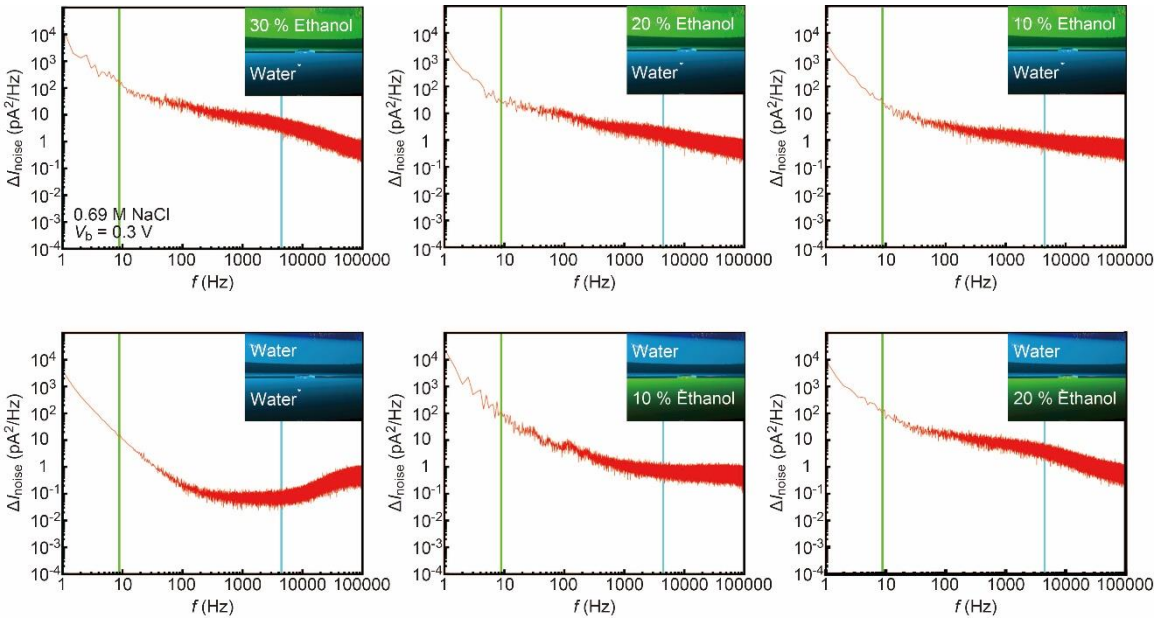

Figure S14. Ionic current noise spectra in a 100 nm-sized nanopore under ethanol gradients at 0.69 M NaCl. Green and blue lines point to the noise intensities at the frequency f = 100 Hz and 10000 Hz, respectively.